Fluid Phase Equilibria 534 (2021) 112960

Contents lists available at ScienceDirect

Fluid Phase Equilibria

journal homepage: www.elsevier.com/locate/fluid

Two-phase flash for tight porous media by minimization of the Helmholtz free energy

Sofiane Haythem Achour, Ryosuke Okuno*

Department of Petroleum and Geosystems Engineering, The University of Texas at Austin, 200 E. Dean Keeton Street, Stop C0300, Austin, Texas 78712, United States

ARTICLE INFO

Article history:
Received 20 September 2020
Revised 21 December 2020
Accepted 11 January 2021
Available online 14 January 2021

Keywords:
Helmholtz free energy
Capillary pressure
Flash calculation
Equation of state
Indefinite solution

ABSTRACT

Thermodynamic modeling of phase behavior is one of the most fundamental components in the study of enhanced oil recovery by gas injection. Robust algorithms exist for multiphase equilibrium problems with no capillary pressure as commonly used in compositional reservoir simulation. However, various convergence problems have been reported even for simple two-phase split problems in the presence of capillary pressure by using the traditional algorithm based on minimization of the Gibbs free energy. In this research, the phase-split problem with capillary pressure is formulated by using the Helmholtz free energy for a given temperature and total volume. The algorithm is based on the successive substitution (SS) for updating K values, which is coupled with the volume update by using the pressure constraint equation. The robustness of the SS algorithm is improved by using the convexity information of the Helmholtz free energy and using an under-relaxation method. Case studies present phase-split problems with capillary pressure by using the developed algorithm and highlight several advantages of using the Helmholtz free energy over the Gibbs free energy. The improved robustness comes mainly from the involvement of a single energy surface regardless of the number of phases. The pressure variability that occurs during the phase-split calculation with capillary pressure is inherent in the Helmholtz free energy in volume space.

1. Introduction

Gas injection has been studied and implemented to improve the oil recovery in tight reservoirs [1-3]. An optimal application of gas injection should be designed based on a fundamental understanding of in-situ phase behavior and its interplay with multicomponent transport phenomena in tight porous media. Among many other factors, capillary pressure affects in-situ phase behavior more likely in tight reservoirs than in conventional reservoirs. However, it is not yet common practice to include the effect of capillary pressure on phase behavior in equation-of-state (EOS) compositional simulation of gas injection in tight reservoirs.

Phase equilibrium calculations using an EOS consist of phase-stability and phase-split calculations. The traditional formulations and algorithms are based on minimization of the Gibbs free energy at a given temperature and pressure subject to material balance [4-5]. Therefore, phase equilibrium calculations in the presence of capillary pressure have been studied by a natural extension of the traditional approach by considering different pressures for the equilibrium phases [6-8]. For example, a two-phase split algorithm involves minimization of the total Gibbs free energy of two phases that have different pressures. The iterative solution of such a phase-split problem is often challenging because the phase compositions lie on two different Gibbs free energy surfaces in composition-pressure space. Since the capillary pressure is part of the solution, the relative location of one Gibbs free energy surface changes with respect to the other surface during the iteration. This complexity is coupled with the non-linearity of the Gibbs free energy that by itself causes various convergence problems even for the traditional phase-split calculation with no capillary pressure in compositional flow simulation.

Various types of convergence problems have been reported with the methods using the Gibbs free energy. For example, Neshat et al. [9] showed that a non-physical part of the Gibbs free energy (e.g., the vapor side of the Gibbs free energy at a liquid-phase pressure) caused the traditional stability analysis method to converge to a wrong solution. A meta-stable part of the Gibbs free energy can also make it invalid to use the traditional criterion for the root selection of a cubic EOS as demonstrated by Neshat et al. [8].

Another example is related to the existence of a limiting capillary pressure above which no solution exists for a two-phase split calculation. In the case of vapor-liquid equilibrium with a

* Corresponding author.
E-mail address: okuno@utexas.edu (R. Okuno).

https://doi.org/10.1016/j.fluid.2021.112960
0378-3812/

Nomenclature

Roman symbols

a	Interfacial area
a_m	Mixture attraction parameter obtained from van der Waals mixing rules
A	Helmholtz free energy
b_i	Co-volume parameter for the Peng-Robinson equation of state
b_m	Mixture co-volume parameter obtained from van der Waals mixing rules
d_i	Molar density for component i
c	User specified constant in our algorithm
D_T	Tangent plane distance to A/VRT defined in Eq. (24)
E	Volume balance equation
f_{ij}	Fugacity of component i in phase j
F_i	Stationarity equation i
F	Vector containing values of stationarity equations
g_i	Function used in general SS iteration to update the ith independent variable
g	Vector containing functions used in general SS iteration
$\bar{G}_{ij}$	Partial molar Gibbs free energy of component i in phase j
G	Gibbs free energy
J	Jacobian matrix containing the derivatives of the SS iteration functions
K_{ij}	K-value of component i in phase j
N_c	Number of components
N_p	Number of phases
N_i	Number mole of component i in a mixture
N	Vector containing number mole of each component in a mixture
P_j	Pressure of phase j
P_c	Critical pressure
P_{cap}	Capillary pressure
$\mathcal{P}_{cap}$	Capillary pressure function
r	Residuals used to determine convergence
R	Ideal gas constant
t_i	ith independent variable for general SS iteration
t	Vector containing independent variables for general SS iteration
T	Temperature
T_c	Critical temperature
V	Volume
$\underline{V}$	Molar volume
$\underline{v}$	Molar volume of the less dominant phase
$\bar{V}_i$	Partial molar volume for component i
x_{ij}	Mole fraction for component i in phase j
$\mathbf{x}_j$	Vector containing the mole fractions for each component in phase j

Greek letters

α	Under-relaxation constant
ε	Tolerance for convergence criterion or small pressure value
β_j	Phase mole fraction of phase j
δ_1	Constant parameter in general cubic equation of state
δ_2	Constant parameter in general cubic equation of state
δ_i	Independent variable used for the Hessian of A/VRT
$\boldsymbol{\delta}$	Vector containing independent variables used for the Hessian of A/VRT
ζ	Under-relaxation constant
λ	Eigenvalue of a given matrix
σ	Interfacial tension or other interfacial property when used as a subscript
ϕ_{ij}	Fugacity coefficient of component i in phase j

Superscripts

k	Outer loop iteration step index
pk	Inner loop iteration steps index used in Step 6.1
bk	Inner loop iteration steps index used in Step 7
*	Variable or function in the vicinity of the solution
′	Property of an under-relaxed algorithm

Subscripts

B	Bissection
d	Dominant
In	Initialization
l	Lower limit of a bisection interval
L	Liquid
lim	Limit of the physical domain
max	Maximum
r	Reference
SP	Stationary point of the TPD
u	Upper limit of a bisection interval
V	Vapor

Abbreviations

EOS	Equation of state
PR	Peng-Robinson
SS	Successive substitution
VL	Vapor-liquid

liquid-wet surface, such a limiting capillary pressure occurs when the equilibrium liquid phase is located on the spinodal boundary [7,10]. Such a two-phase problem with no solution may be avoided by limiting the capillary pressure to a certain value (e.g., a value corresponding to a 10-nm tube) [7,11-14]. However, it is desirable to identify whether there is a solution to the specified thermodynamic problem.

The convergence problems reported in the literature indicate that the traditional minimization of the Gibbs free energy may not be the most suitable formulation for the phase-split problem with capillary pressure. It involves N_P surfaces of the Gibbs free energy, where N_P is the number of equilibrium phases. This is a substantial complexity because (N_P – 1) surfaces move with respect to the Gibbs free energy surface for the reference phase in composition space during the iterative solution. A potential solution to the problems described above is to reformulate the problem as minimization of the Helmholtz free energy for a given temperature and volume, in which the variability of phase pressures is inherently included in the function to be minimized.

Achour [15] and Achour and Okuno [16] presented a new formulation and algorithm for phase stability analysis with capillary pressure by minimization of the Helmholtz free energy. Various advantages of using only one energy surface were demonstrated. For example, the failure of the stability analysis because of the non-physical part of the Gibbs free energy does not occur with the formulation and algorithm using the Helmholtz free energy. The main reason is that it involves only one energy surface regardless of N_P. The next question to be addressed in this research is whether the phase-split problem with capillary pressure can be more robustly solved by using the Helmholtz free energy.

The Helmholtz free energy was recently used for phase-split calculations including capillary pressure. Lu et al. [17] adapted the SS algorithm of Mikyška and Firoozabadi [18] to include the cap-

illary pressure. Kou and Sun [19] also applied their previous flash calculation algorithm [20] to include capillary pressure. Sandoval et al. [21] discussed the advantage of using the variable space of the Helmholtz free energy that simplifies the derivatives of volume-explicit capillary pressure models. However, it is not clear in the literature whether use of the Helmholtz free energy can improve various convergence problems with the traditional phase-split methods using the Gibbs free energy.

Jindrová and Mikyška [22] and Lu et al. [17] reported convergence issues of the SS algorithm based on the Helmholtz free energy. However, they did not present a detailed analysis of the convergence issues and only proposed to use an ad-hoc under-relaxation [17] and other numerical methods [22].

This paper presents a new algorithm for phase-split calculations for tight porous media using the Helmholtz free energy. Case studies demonstrate the improved robustness of two phase-split calculations because of using the Helmholtz free energy.

2. Formulation and algorithm

This section first presents the formulation for phase-split calculation including capillary pressure by using the Helmholtz free energy. Then, it introduces the algorithm used to solve the formulated problem by using the traditional SS method with several important modifications. As will be shown in this paper, the main advantage of using the Helmholtz free energy for phase-split calculation with capillary pressure is that only one smooth energy surface is involved in the calculation regardless of N_P. In contrast, the traditional phase-split methods inherently involve multiple Gibbs free energy surfaces that are sometimes first-order discontinuous. Using only one energy surface makes it possible to furnish a technique to confirm an indefinite situation, in which the fluid is unstable but does not have a valid two-phase solution. The algorithm presented here is designed to take this advantage of the formulation using the Helmholtz free energy.

2.1. Phase stability analysis with the Helmholtz free energy

The first and second laws of thermodynamics require that the Helmholtz free energy of the system be minimized for an equilibrium state at a specified temperature T, volume V, and number moles N_i of N_C components ($i = 1, \ldots, N_C$) subject to material balance. With these thermodynamic specifications, a vapor-liquid (VL) equilibrium state of the system requires

$$dA = dA_V + dA_L + dA_\sigma \tag{1}$$

to be zero, where A, A_V, A_L, and A_σ are the Helmholtz free energies of the total system, the V phase, the L phase, and the interface, respectively. The change in Helmholtz free energy is

$$dA_j = -S_j dT_j - P_j dV_j + \sum_{i=1}^{N_C} \bar{G}_{ij} dN_{ij} \tag{2}$$

for phase j (j = V and L),

$$dA_\sigma = -S_\sigma dT_\sigma - P_\sigma dV_\sigma + \sigma da + \sum_{i=1}^{N_C} \bar{G}_{i\sigma} dN_{i\sigma} \tag{3}$$

for the interface. In Eqs. (2) and (3), S is entropy, P is pressure, σ is interfacial tension, a is interfacial area, and $\bar{G}_i$ is the partial molar Gibbs free energy for component i ($i = 1, \ldots, N_C$).

The minimization of the Helmholtz free energy is subject to the material balance constraints on the number of moles for each component

$$dN_{iL} + dN_{iV} + dN_{i\sigma} = 0, \quad \text{where } i = 1, \ldots, N_C, \tag{4}$$

the total volume constraint

$$dV_L + dV_V + dV_\sigma = 0, \tag{5}$$

and the temperature constraint

$$dT_L = dT_V = dT_\sigma = 0. \tag{6}$$

The minimization of the Helmholtz free energy is also constrained by the positivity of the mole numbers for both phases

$$0 \le N_{iL} \le N_i, \quad \text{where } i = 1, \ldots, N_C, \tag{7}$$

and minimum molar volume for both phases

$$V_j \ge V_{lim,j}, \quad \text{where } j = L, V. \tag{8}$$

Cubic equations of state usually evaluate the minimum volume $V_{lim,j}$ as

$$V_{lim,j} = \sum_{i=1}^{N_C} b_i N_{ij}, \tag{9}$$

where b_i is the co-volume parameter for component i ($i = 1, \ldots, N_C$).

Using Eqs. (4)-(6), Eq. (1) can be written as

$$dA = -(P_V - P_L)dV_V - (P_\sigma - P_L)dV_\sigma + \sigma da + \sum_{i=1}^{N_C} \left(\bar{G}_{iV} - \bar{G}_{iL}\right) dN_{iV} + \sum_{i=1}^{N_C} \left(\bar{G}_{i\sigma} - \bar{G}_{iL}\right) dN_{i\sigma}. \tag{10}$$

Eq. (10) is simplified by assuming the changes in volume and component's mole number for the interface are negligible in comparison to the other terms; that is,

$$dA = -(P_V - P_L)dV_V + \sigma da + \sum_{i=1}^{N_C} \left(\bar{G}_{iV} - \bar{G}_{iL}\right) dN_{iV}. \tag{11}$$

The stationarity condition for the minimization of the Helmholtz free energy is that $dA = 0$ at the VL equilibrium; i.e.,

$$\bar{G}_{iV} - \bar{G}_{iL} = 0, \tag{12}$$

or the widely used fugacity equations

$$F_i = \ln(f_{iL}) - \ln(f_{iV}) = 0 \tag{13}$$

in $\mathbf{N_V}$ space, where $i = 1, \ldots, N_C$. In Eq. (13), f_{iL} and f_{iV} are the fugacities of component i ($i = 1, \ldots, N_C$) in the L and V phases, respectively. Eq. (12) (or 13) makes the following condition for $dA = 0$:

$$F_{N_C+1} = P_V - P_L - P_{cap} = 0 \tag{14}$$

in V_V. Note that $P_{cap} = \sigma da/dV_V$ at equilibrium (i.e., when Eq. (13) is satisfied). The capillary pressure can be estimated by using a capillary pressure model (e.g., the Young-Laplace and saturation-based models) or by giving a numerical value.

In summary, the phase-split calculation for a VL equilibrium state is to find $\mathbf{N_V}$ and V_V such that $\mathbf{F} = \mathbf{0}$, given $\mathbf{F} \in \mathbb{R}^{N_C+1}$ at T, V, and $\mathbf{N}$ with a specified value or function for capillary pressure. Obviously, ($\mathbf{N_V}$, V_V) can be changed to ($\mathbf{N_L}$, V_L) with no loss of generality in the formulation. The algorithm used for this problem is presented in the next subsection.

2.2. Algorithm

The algorithm is based on the SS method [17-18,23], in which each iteration contains two mains steps: the composition update through one SS step by using Eq. (13) and the volume update by using Eq. (14). The composition update is based on the traditional method of Rachford and Rice [24] that solves Eq. (13) for $\ln K_i$

$$\ln K_i = \ln x_{iV} - \ln x_{iL} \tag{15}$$

along with the material balance

$$z_i = \sum_{j=1}^{N_P} \beta_j x_{ij}, \tag{16}$$

where z_i is the overall concentration of component i, β_j is the mole fraction of phase j, x_{ij} is the concentration of component i in phase j, and N_P is the number of phases (j = L and V, and $N_P = 2$ in this research). The Rachford-Rice routine used in this research is described in Okuno et al. [25]. The volumes are updated through the solution of the pressure equation, subject to the volume balance.

Then, the main structure of the algorithm is to find $\ln K_i$ (i = 1, 2, ..., N_C) and $\underline{V}_V$ (or $\underline{V}_L$) such that $\mathbf{F} = \mathbf{0}$, given $\mathbf{F} \in \mathbb{R}^{N_C+1}$ at T, V, and **N** with a specified value or function for capillary pressure, while ensuring that the lower-pressure phase is intrinsically stable. The intrinsic stability condition is numerically verified that the Hessian matrix of A_L/VRT is positive definite through a Cholesky decomposition (If the square root of a negative number is encountered in the Cholesky decomposition, then the original matrix is not positive definite).

A concise description of the sequential iteration scheme is presented below, which is followed by some specific details of Steps 1, 2, 4, 5, 6, and 7 in sub-Sections 2.2.1 through 2.2.4. Appendix A shows a flowchart of the algorithm.

Step 1. Initialize **lnK** and **V**. Use the stability analysis if the reference phase is intrinsically stable; otherwise, use Wilson's correlation at the specified total molar volume.

1.1 Compute the Hessian matrix of Ar/VRT and check the positive definiteness through a Cholesky decomposition. Subscript "r" represents the reference phase.
1.2 If the Hessian matrix is positive definite, perform the stability analysis [15-16]. If the reference phase is stable, stop. Otherwise, set the initial guess for the L and V phases to the compositions and molar volumes of the reference phase and stationary point (SP) of the TPD.
1.3 If the Hessian matrix is not positive definite, then compute the initial guess for lnK based on Wilson's correlation and use bisection to determine the pressure that satisfies the total molar volume specification.
1.4 Initialize the iteration index k: k ← 1.

Step 2. Compute the under-relaxation factor ζ .

Step 3. Compute $\ln P\phi_L^k$ and $\ln P\phi_V^k$.

Step 4. Update the capillary pressure.

4.1 Use a capillary pressure model to compute $\mathcal{P}_{cap}^k$.
4.2 Update the capillary pressure $(P_{cap})^k \leftarrow (1-\zeta)(P_{cap})^{k-1} + \zeta \mathcal{P}_{cap}^k$.

Step 5. Update the phase compositions.

5.1 Update lnK by using a SS step $(\ln K_i)^k \leftarrow (1-\zeta)(\ln K_i)^{k-1} + \zeta(\ln\phi_{iL}P_L - \ln\phi_{iV}P_V)$.
5.2 Solve the Rachford-Rice equations for the phase compositions $\mathbf{x}_L^k$ and $\mathbf{x}_V^k$, and the phase molar fractions β_L^k and β_V^k.

Step 6. Update the phase molar volumes

6.1 Solve Eq. (14) using Newton's method.
6.2 If the iterative molar volume violates the physical condition of Eq. (8), then update the molar volume by using a first-order Taylor series approximation.

Step 7. If the lower-phase pressure is intrinsically unstable, then use bisection to reduce its molar volume until it lies on the limit of intrinsic stability (spinodal boundary).

Step 8. Check for convergence. If $\max_{i<Nc}\{|F_i|\} < \varepsilon_{ss}$, then stop. Otherwise, k ← k + 1 and return to step 2. In this research, $\varepsilon_{ss}$is set to 10^{-10}.

2.2.1. Initialization

When the Hessian matrix of the Helmholtz free energy is positive-definite at the overall composition, the composition and molar volume of the new phase are initiated by the stationary point (SP) of the TPD. The mole fractions of the reference and incipient phases are respectively set to $(1-\varepsilon_1)$ and ε_1. ε_1 must be a small positive number to compute a valid initial guess for the volume update in step 6.1 as will be further explained in Section 2.2.3.In this research,$\varepsilon_1$is set to 10^{-5}. Also, the phases need to be identified to use the capillary pressure model. Many methods can be used for this purpose [26-27]. We have found that it is robust to use a comparison of the mixture covolume parameters given by the van der Waals mixing rules [28], as follows:

If $b_r > b_{SP}$, then the reference phase is L and the incipient phase is V;

Otherwise, the reference phase is V and the incipient phase is L; where b_r and b_{SP} are the covolume parameters at the reference composition and SP of the TPD, respectively.

When the Hessian matrix of the Helmholtz free energy is not positive definite at the overall composition, the fluid is unstable. Then, Wilson's correlation [29] is used to initialize K-values. Bisection iterations are used to find the pressure that yields the specified total molar volume

$$\beta_L \underline{V}_L + \beta_V \underline{V}_V - \underline{V}_r = 0, \tag{17}$$

within the pressure range $[(\sum_{i=1}^{N_c} \frac{z_i}{P_i^{vap}})^{-1}, \sum_{i=1}^{N_c} z_i P_i^{vap}]$. This procedure is robust assuming that the total molar volume given by the constant K-flash calculations using Wilson's correlation decreases monotonically with increasing pressure.

The detailed substeps for step 1.2 are then as follows:

1.2.1 Use Wilson's correlation [29] to estimate the bubble point P_{bbl} and the dew point P_{dew} as the upper and lower limits of the phase pressure for the bisection interval.
1.2.2 Solve the Rachford-Rice equations, solve the cubic EOS, and compute the total molar volumes $\underline{V}_u$ and $\underline{V}_l$ at P_{bbl} and P_{dew}.
1.2.3 If the specified molar volume is not within the bisection interval $[\underline{V}_u, \underline{V}_l]$, set the composition and molar volumes to the closest edge of the bisection interval, and go to step 1.3.
1.2.4 Compute the pressure of the reference phase P_r. If $P_{bbl} > P_r > P_{dew}$, then set the phase pressures to P_r. Otherwise, set the pressure to the middle of the bisection interval.
1.2.5 Use Wilson's correlation [29] to estimate K-values.
1.2.6 Solve the Rachford-Rice equations for $\mathbf{x}_L$, $\mathbf{x}_V$, β_L, and β_V.
1.2.7 Solve the cubic EOS and compute the total molar volume.
1.2.8 $|(\underline{V}_l - \underline{V}_u)/\underline{V}_r| < \varepsilon_{ln}$, go to step 1.3. Otherwise, update the bisection interval and pressure. In this research, ε_{ln} is set to 10^{-2}.

2.2.2. Under-relaxation for K-values and capillary pressure

Jindrová and Mikyška [22] found a difficult case with a binary mixture, for which the outer-loop iterations of their SS algorithm diverged no matter how close the initial guess was to the solution their SS algorithm was initiated. Similarly, Lu et al. [17] encountered convergence issues with their SS algorithm because of "improper updating of K_i values." They found an optimal way of improving the convergence behavior with the following under-relaxation on K values:

$$K_i^{k+1} = \zeta g_i\left(K_i^k\right) + (1-\zeta)K_i^k, \tag{18}$$

where i = 1, ..., N_C, $g_i(K_i^k)$ is the function which returns the full SS step for K_i, and ζ was an under-relaxation factor set to 0.5. Cases

have been found in this research, where $\zeta = 0.5$ was not small enough for the SS algorithm to converge.

This subsection presents an under-relaxation scheme for the capillary pressure and K-value update (Steps 4 and 5) that ensures convergence of the outer-loop of the flash algorithm. Heidemann and Michelsen [30] analyzed the convergence behavior of the traditional SS algorithm for isobaric-isothermal flash (the solution of Eq. (13) for $\ln K_i$). The general form of the SS iteration equation is derived by rewriting the equations to be solved $\mathbf{F} = \mathbf{0}$ as

$$\mathbf{t}^{k+1} = \mathbf{g}\left(\mathbf{t}^{k}\right), \tag{19}$$

where k is the iteration index, $\mathbf{t}$ is a vector of N independent variables and $\mathbf{g}$ is a function for mapping $\mathbb{R}^N$ onto $\mathbb{R}^N$. Then, the convergence behavior of the traditional SS algorithm in the vicinity of the solution [i.e., $\mathbf{t}^* = \mathbf{g}(\mathbf{t}^*)$] is dominated by the largest eigenvalue (in absolute value) $|\lambda_d|$ of the Jacobian matrix of $\mathbf{g}$ with respect to $\mathbf{t}$ [4]. When $|\lambda_d| < 1$, the SS algorithm is guaranteed to converge [30]. In this study, the dominant eigenvalue, λ_d, is estimated using the power method, where the initial guess for the dominant eigenvector-eigenvalue pair can be taken as the converged values in the previous phase-split iteration.

We apply Heidemann and Michelsen's procedure for analyzing the SS algorithm for isothermal-isochoric (TV) flash. The Jacobian matrix contains the derivatives of $\mathbf{g} \in \mathbb{R}^{N_C+1}$ with respect to $\mathbf{t} \in \mathbb{R}^{N_C+1}$, where

$$g_i = \ln(K_i) + \ln(f_{iL}) - \ln(f_{iV}) \text{ for } i = 1, 2, \ldots, N_C, \tag{20}$$

$$g_{N_c+1} = \mathcal{P}_{cap}\underline{V}_r/RT, \tag{21}$$

$$t_i = \ln(K_i) \text{for } i = 1, 2, \ldots, N_C \tag{22}$$

$$t_{N_C+1} = P_{cap})\overline{V}_r/RT. \tag{23}$$

P_{cap} is equal to the difference in the phase pressures at a given iteration, and $\mathcal{P}_{cap}$ is the capillary pressure calculated using the capillary pressure model with iterative phases. When under-relaxation is used, these two variables are not equal except at the converged solution. P_{cap} and $\mathcal{P}_{cap}$ are multiplied by $\underline{V}_r/RT$ in Eqs. (21) and (23) to avoid computing ill-conditioned jacbian matrices.

Appendix B shows the analytical expression for $\mathbf{J} \in \mathbb{R}^{(N_C+1)\times(N_C+1)}$. Note that as opposed to the Jacobian matrix for the isobaric-isothermal (PT) SS algorithm, the derivatives are taken assuming a constant total volume, instead of a constant pressure, for $\partial g_i/\partial t_j$ for i =1, 2,...., N_C and j = 1, 2,... N_C. This different constraint results in the additional $\mathbf{B}$ matrix in the $\mathbf{S}$ matrix block of the Jacobian. The Jacobian matrix presented here also departs from that of the PT flash because of the $N_{C+1}{}^{th}$ column and row.

Heidemann and Michelsen [30] explained that $\lambda_d > 1$ occurs in saddle-shaped regions or local maxima of the Gibbs free energy. In these cases, the SS algorithm with no under-relaxation diverges from the saddle point until it reaches the neighborhood of a minimum of the Gibbs free energy to which it then converges. $\lambda_d > 1$ also allows the TV flash calculations to avoid converging to local maxima or to saddle points of the Helmholtz free energy.

Furthermore, Heidmann and Michelsen [30] showed that $\lambda_d < -1$ could occur with flash calculations for polar species causing a high degree of non-ideality. Then, iterates tend to oscillate back and forth and diverge from the solution no matter how close the initial guess is to the solution. They proposed to use a "damping factor" ζ for updating the logarithm of the K-values as shown in step 5.1 of the algorithm above.

The under-relaxation has the effect of directly transforming all the eigenvalues λ_i $(i = 1, \ldots, N_c)$ of the Jacobian into λ_i', where

$$\lambda_i' = 1 - \zeta(1 - \lambda_i). \tag{24}$$

Eq. (24) applies to the dominant eigenvalue $\lambda_d : |\lambda_d| = \max_{i=1,\ldots,N_C+1} |\lambda_i|$. This makes it possible to select an appropriate under-relaxation factor that satisfies $|\lambda_d'| < 1$. Heidmann and Michelsen [30] noted that excessive damping should be avoided as it could make the eigenvalues λ_i' closer to 1, resulting in slower convergence [30]. It is also undesirable to set λ_d' to -1 as that would result in non-convergence.

The damping factor is also used to generalize the updating scheme for P_{cap} as shown in step 4.2. The under-relaxation factor is computed by setting λ_d' equal to -0.9 as shown below in step 2.3. This under-relaxation is only necessary if $\lambda_d < -0.9$, otherwise $\zeta = 1$.

It is sometimes necessary to further decrease the under-relaxation factor in the initial iterations. As noted by Orbach and Crowe [31], the convergence behavior is only dictated by the dominant eigenvalue in proximity to the solution. However, the initialized variables are often far from the final solution. To avoid divergence of the algorithm during the early iterations, the under-relaxation factor is multiplied by a safety factor shown in step 2.4 as shown below.

The detailed substeps for Step 2 are then as follows:

2.1 If the L phase was found to be intrinsically unstable at the end of the previous outer loop iteration, compute the Jacobian matrix J using Appendix C. Otherwise, compute J using Appendix B.
2.2 Use the power method to compute the dominant eigenvalue λ_d of J.
2.3 If $\lambda_d < -0.9$, set $\zeta \leftarrow 1.9/(1 - \lambda_d)$. Otherwise, $\zeta \leftarrow 1$.
2.4 If maxi<Nc {|Fi|} < 0.1, $\zeta \leftarrow 0.5\zeta$; else if maxi<Nc {|Fi|} < 10−3, set
2.5 $\zeta \leftarrow 0.25\zeta(1 - \log_{10}(\max_{i<N_c}\{|F_i|\}))$.

Section 2.2.4 explains why a different Jacobian matrix from that of Appendix B is needed to compute the relaxation factor when the liquid phase is found to be intrinsically unstable in the previous iteration. The analytical expression of $\mathbf{J}$ to compute the under-relaxation factor in these cases is given in Appendix C.

2.2.3. Volume update

In step 6.1, the phase molar volumes are updated by solving Eq. (14), sometimes called "pressure equation." Mikyška and Firoozabadi [18] proposed a bisection method by using phase saturations with the upper and lower bounds being 0 and 1. Nichita [23] pointed out that this domain could result in a violation of the condition given by Eq. (8). Also, Lu et al. [17] showed that Eq. (14) had multiple roots, and used an exhaustive search method for a pair of the roots that minimize the total Helmholtz free energy of the V and L phases.

It is easy to show that Eq. (14) can have up to six roots. Eq. (14) can be rewritten by using the general form of a cubic equation of state as

$$F_{N_C+1} = \frac{RT}{\underline{V}_V - b_V} - \frac{a_V}{\left(\underline{V}_V^2 + 2b_V\underline{V}_V - b_V^2\right)} - \frac{RT}{\underline{V}_L - b_L} + \frac{a_L}{\underline{V}_L^2 + \underline{V}_L b_L - b_L^2} - P_{cap} = 0, \tag{25}$$

where $\underline{V}_L$ and $\underline{V}_V$ are the molar volumes, b_L and b_V are the co-volume parameters, a_L and a_V are the attraction parameters of the L and V phases, respectively. The volume constraint gives $\underline{V}_L = (\underline{V} - \underline{V}_V\beta_V)/\beta_L$ and then, Eq. (25) can be expressed as a polynomial of degree six.

In this research, Newton's method is applied to solve Eq. (14) with the following variable:

$$q = \overline{)v}_{lim}/\left(\overline{()v} - \overline{)v}_{lim}\right), \tag{26}$$

where $\underline{v}$ is the molar volume of the less dominant phase (i.e., the phase with a smaller β value), and v_{lim} is the molar volume of the less dominant phase at the closest limit of the domain defined by Eq. (8) along with the volume constraint. Here, the closest limit is $\underline{V}_{lim,j}$ where phase j is the one with the smallest $\underline{V}_j/\ \underline{V}_{lim,j}$ (j = L, V). Use of q as the independent variable results in more robust and rapid solution of Eq. (14) than using $\underline{v}$. The derivative of Eq. (25) with q is $\partial F_{N_c+1}/\partial q = -(\frac{\beta_V}{\beta_L} dP_L/d\underline{V}_L - dP_V/d\underline{V}_V)(\underline{v} - \underline{v}_{lim})/Q$ if the liquid phase is the dominant one. Otherwise, $\partial F_{N_c+1}/\partial q = (\frac{\beta_L}{\beta_V} dP_L/d\underline{V}_L - dP_V/d\underline{V}_V)(\underline{v} - \underline{v}_{lim})/Q$.

This solution finds a local root for each phase which depends on the value from the previous iteration step (if k > 2) or the initialization from Step 1 (if k = 1). Therefore, it is important to obtain a physically correct root in Step 1 that results in the lowest Helmholtz free energy. An interesting problem associated with the traditional root selection based on the Gibbs free energy is illustrated in Section 3.2.

The detailed substeps for the molar volume update in step 6.1 are as follows:

6.1.1 Determine the identity of the dominant phase.
6.1.2 Compute the closest limit of the molar volume domain $\underline{v}_{lim}^k$.
6.1.3 Compute the initial guess for the independent variable $q = \underline{v}_{lim}^{k-1}/(\underline{v}^{k-1} - \underline{v}_{lim}^{k-1})$
6.1.4 Compute the phase molar volumes.
6.1.5 Set pk ← 1.
6.1.6 Compute the pressure and isothermal compressibility for both phases using the EOS.
6.1.7 Compute the pressure equation F_{N_c+1} and the derivative of the pressure equation $(\partial F_{N_c+1}/\partial q)$.
6.1.8 Update q using a Newton iteration $q^{pk+1} \leftarrow q^{pk} - F_{N_c+1}/(\partial F_{N_c+1}/\partial q)$.
6.1.9 Compute the phase molar volumes. If the molar volume of the L or V phase is not within the physical limit defined by Eq. (8), then use the volume update of step 6.2 instead.
6.1.10 If $|F_{N_c+1}/(P_V^{k-1} + P_L^{k-1})| > \varepsilon_P$, set pk ← pk + 1 and return to step 6.1.6. Otherwise, continue to Step 7.

In this research, ε_P is set to 10^{-10}. The existence of a correct solution that maintains the phase identity is not always guaranteed. Several examples of challenging cases have been presented by Lu et al. [17]. In this research, when Newton's method fails to converge to a feasible root satisfying Eq. (8), the molar volumes are estimated using a Taylor expansion based on the change in liquid component moles $\Delta N_{iL} = \beta_L^k x_{iL}^k - \beta_L^{k-1} x_{iL}^{k-1}$ $(i = 1, \ldots, N_c)$ and capillary pressure $\Delta P_{cap} \leftarrow P_{cap}^k - P_{cap}^{k-1}$ from the previous iteration. The change in total liquid volume

$$\Delta V_L \leftarrow \sum_{i=1}^{N_c} \bar{V}_{iL} \Delta N_i - \frac{\beta_L/\left(\frac{dP}{d\underline{V}_L}\right)}{\beta_L/\left(\frac{dP}{d\underline{V}_L}\right) + \beta_V/\left(\frac{dP}{d\underline{V}_V}\right)} \left(\beta_V/\left(\frac{dP}{d\underline{V}_V}\right)\Delta P_{cap} + \sum_{i=1}^{N_c}\left(\bar{V}_{iL} - \bar{V}_{iV}\right)\Delta N_i\right) \tag{27}$$

gives a change in total vapor volume $\Delta V_V = -\Delta V_L$ and a change of liquid molar volume $\underline{V}_L^k = (\underline{V}_L^{k-1}\beta_L^{k-1} + \Delta V_L)/\beta_L^k$. The molar volume for the V phase is determined through the volume balance $\underline{V}_V^k = (V_{ref} - \underline{V}_L^k \beta_L^k)/\beta_V^k$. If the feasibility Eqs. (8) and (9) are not satisfied for both phases, Δn_{iL} and ΔP_{cap} are halved until the phase equilibrium can pass the feasibility test.

The detailed substeps of step 6.2 for the volume update when Newton's method fails are as follows:

6.2.1 Compute the change in liquid component moles $\Delta N_{iL} \leftarrow \beta_L^k x_{iL}^k - \beta_L^{k-1} x_{iL}^{k-1}$.
6.2.2 Compute the change in capillary pressure $\Delta P_{cap} \leftarrow P_{cap}^k - P_{cap}^{k-1}$.
6.2.3 Estimate the change in liquid volume using a truncated first-order Taylor series extrapolation using Eq. (27).
6.2.4 Compute the phase molar volumes $\underline{V}_L^k \leftarrow (\underline{V}_L^{k-1}\beta_L^{k-1} + \Delta V_L)/\beta_L^k$ for the L phase and,
6.2.5 $\underline{V}_V^k \leftarrow (\underline{V}_V^{k-1}\beta_V^{k-1} - \Delta V_L)/\beta_V^k$
6.2.6 If $\underline{V}_V^k > b_V$ and $\underline{V}_L^k > b_L$, then halve the liquid component moles step size Δn_{iL} and capillary pressure step size and return to step 6.2.3. Otherwise, continue to Step 7.

2.2.4. Capillary pressure overshoot detection and correction

The phase equilibrium problem with a capillary pressure can result in an indefinite situation in which the fluid of interest is unstable, but has no two-phase solution. This indefinite situation arises when the capillary pressure is greater than the limit at which the liquid-phase composition is located at a spinodal point on the Helmholtz (or Gibbs) free energy [7,10]. This can occur during the iterative solution when the iterative capillary pressure exceeds the limiting value. A graphical explanation of indefinite solutions is given in Sections 3.3 and 3.4.

In the algorithm used in this research, Step 7 checks for any intrinsic instability of the iterative lower-pressure phase. This is done through the Cholesky decomposition of the Hessian matrix of A/VRT in $\boldsymbol{\delta}$ space, in which $\delta_i = 2\sqrt{N_i/V}$ (i = 1, 2,....,N_C), for each phase [15-16,32]. If the Hessian matrix is non-positive definite for either phase, the molar volume of the lower-pressure phase is decreased until the Hessian at the lower-pressure phase is positive definite. Assuming that the lower-pressure phase has a positive-definite Hessian of A_L/VRT at $\underline{V}_L = b_L(1+\varepsilon_2)$, $\underline{V}_L$ can be readjusted using a bisection in the interval $[b_L(1+\varepsilon_2), \underline{V}_L]$, where ε_2 is a small number to be chosen by the user. This assumption is valid for LV mixtures characterized by closed type-I phase envelopes [33-34]. Then, the iterative capillary pressure is recalculated as the difference in pressure at the limit of instability of the lower-pressure phase. No adjustment is made for the updated P_{cap}, if no eigenvalue is negative for the Hessian matrix of the A_L/VRT function for the lower-pressure phase.

The substeps of Step 7 for the capillary overshoot detection and correction are the following:

7.1 Compute the Hessian matrix of AL/VRT and check to see if it is positive definite through a Cholesky decomposition. If the Hessian is positive definite, then go to Step 8.
7.2 Set the lower limit of bisection to $\underline{V}_l \leftarrow b_L(1+\varepsilon_2)$, the upper limit to $\underline{V}_u \leftarrow \underline{V}_L^k$, the initial liquid molar volume $\underline{V}_L^k \leftarrow (\underline{V}_l + \underline{V}_u)/2$, and initialize the iteration counter bk ← 1.
7.3 Compute the Hessian of AL/VRT and check to see if it is positive definite through a Cholesky decomposition.
7.4 If the Cholesky decomposition succeeds, then set bk ← bk + 1, $\underline{V}_l \leftarrow \underline{V}_L^k$. Otherwise, set $\underline{V}_u \leftarrow \underline{V}_L^k$.
7.5 If $|(\underline{V}_u - \underline{V}_l)/\underline{V}_L^k| > \varepsilon_B$, then return to step 7.4. Otherwise, continue to Step 8.

In this research, ε_B and ε_2 are set to 10^{-10} and 10^{-5}, respectively. This method uses the geometry of the Helmholtz free energy to update the molar volume instead of the solution to the pressure equation. Therefore, a different Jacobian **J** for SS is needed to analyze and ensure the convergence of the algorithm in Step 2. The derivation and analytical expression of this Jacobian are given in Appendix C.

Table 1
Critical properties for the methane/n-decane mixture used for Sections 3.1 and 3.3.

Component	T_c	P_c	Acentric factor	Parachor	Binary interaction parameters	
	K	Bar			C_1	n-C_{10}
C_1	190.7	46.0	0.008	74.05	0	0
n-C_{10}	617.6	21.1	0.49	440.69	0	0

3. Case studies

This section presents case studies to demonstrate the advantage of using the Helmholtz free energy over the Gibbs free energy for phase-split calculations with capillary pressure. The cases are focused on VL equilibrium of hydrocarbon mixtures. The thermodynamic model used is the Peng-Robinson EOS [35] with van der Waals' mixing rules [28]. Volume shift is not used within this research as it affects the fugacity equations when equilibrium phases have different pressures [36]. The Young-Laplace model is used to compute the capillary pressure in case studies 1 through 3, while a saturation-based capillary pressure model is used in case study 4. In each case study, the parachor correlation was used to compute the interfacial tension, using a parachor coefficient of 3.88 [37].

3.1. Case 1: Discontinuity across phase boundaries

The subsection reports a subtle problem associated with the conventional method using the Gibbs free energy. The conventional method is used for a specified pressure and temperature. In the presence of capillary pressure, however, it is not clear which phase should be assigned the specified pressure. It appears that no general solution to this problem has been found without knowing the relativity of the specified thermodynamic conditions to phase boundaries and critical points in pressure-temperature space (e.g., bubble and dew point curves for VL equilibrium). The problem reported here occurs only when the conventional method is used near a bubble-point (dew-point) curve in the presence of capillary pressure with a pressure specified to the V phase (L phase). Nonphysical discontinuities in phase properties can stop the reservoir simulation from proceeding [38]. A fundamental solution to the problem is to use the Helmholtz free energy for a given temperature and total volume, in which phase pressures are part of the solution.

This case study uses the equimolar mixture of methane and n-decane as shown in Table 1**.** Let us consider the traditional phase-split calculation using the Gibbs free energy for this mixture at 394 K and 158.5 bar for a 10-nm tube that is liquid-wet (the contact angle is equal to 0°). Supposing this pressure is the V phase pressure, Fig. 1a shows the Gibbs free energy surfaces at 158.5 bar for the V phase and 152.9 bar for the L phase. That is, the capillary pressure is 5.6 bar. Fig. 1b shows the tangent plane distance function defined at the overall composition (50 mol% methane). The tangent plane distance at the V phase is zero, indicating that this condition is a bubble point for this equimolar mixture at 394 K in a 10-nm tube.

Then, the same calculation is repeated after increasing the pressure to 158.5 + ε bar (in this example, ε is 5.0 × 10^{-3} bar). Fig. 2 presents the tangent plane distance function defined at the overall composition (50 mol% methane; point A in Fig. 2). The stationary point ("SP" in Fig. 2) corresponding to the V phase has a positive tangent plane distance, which indicates that the equimolar mixture is stable at this pressure. Therefore, the calculation concludes that this mixture at 158.5 + ε bar is stable as a single phase. This transition of the phase from the L-phase Gibbs free energy curve (point L in Fig. 1b) to the V-phase Gibbs free energy curve (point B in Fig. 2) across the bubble point occurs because the system is specified by the V-phase pressure. This causes a discontinuity in the L-phase pressure, which in turn results in discontinuous properties of the L phase, such as density, across the bubble point. Consequently, the discontinuity in pressure is equal to the capillary pressure at the bubble point. Note that the single-phase pressure in Fig. 2 cannot be set to 152.9 bar because this pressure is calculated using the phase properties of a non-existent gaseous phase (see the point "SP" in Fig. 2).

Fig. 3 shows the density of the L phase as calculated by minimization of the Gibbs free energy when the V-phase pressure is specified across the bubble point at 394 K. When the system is specified by a V-phase pressure greater than 158.5 bar, the mixture is stable as a single phase, and the pressure is used to compute the density of the stable L phase. The discontinuity in the L-phase pressure between the two hollow circles causes a discontinuity in density from 0.530 g/cc to 0.532 g/cc. Although the gap seems small in this particular example, the problem is general when the conventional method is used with the V-phase pressure specification across a bubble point and with the L-phase pressure specification across a dew point. It is desirable to not have this type of nonphysical discontinuity, especially for application in compositional reservoir simulation. The method using the Helmholtz free energy does not have this problem because the total molar volume is continuous across a phase boundary as demonstrated in Section 3.4.

3.2. Case 2: Root selection for a cubic EOS

A cubic EOS can have two possible roots for each phase during phase-split calculations. "Root selection" refers to a numerical algorithm that identifies the root that leads to the correct convergence of the phase-split calculation. The conventional root selection is to select the root that gives the lower Gibbs free energy for the phase of interest when the phase has two possible roots of the cubic EOS [39]. However, Neshat et al. [8] demonstrated that this traditional criterion is not robust when the two phases have a large capillary pressure.

This case study demonstrates that the root selection problem can be solved by using the Helmholtz free energy. Table 2 shows the fluid properties of the methane/n-butane binary system. Fig. 4 gives the Gibbs free energy curves at 36.0 and 7.41 bar for the equimolar mixture of methane and n-butane at 333 K in a 3-nm capillary tube. In this figure, point "S_1" is the Gibbs free energy for hypothetically single-phase V, and "S_2" is the two-phase VL solution. The Gibbs free energy of the L and V phases are denoted as A and C, respectively. Phases L and V have methane concentrations of 18.4 mol% and 78.1 mol%, respectively. Point B corresponds to the other real root of the EOS for phase L. For this case, the conventional root selection method selects the root with the lowest Gibbs free energy, which is point B. However, that is not the correct root since the lowest value of the total Gibbs free energy (S_2) is found by points A and C. The calculated capillary pressure between the phases at points A and C would be different from that at points A and B due to the difference in phase properties. However, flash calculation algorithms update the capillary pressure at the beginning of each outer-loop iteration and treat it as a constant in the intermediate steps which include the root selection.

This binary system is described by using the Helmholtz free energy (A/VRT) in **d** space, where $d_i = N_i/V = x_i/\underline{V}$ ($i = 1, 2,\ldots,N_C$). Since the curvature of the function is more obvious in tangent-

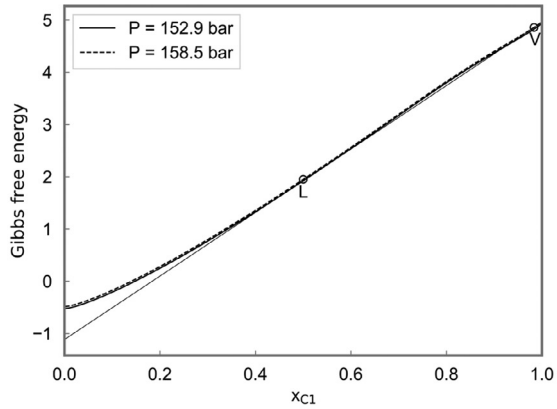

(a) Gibbs free energy for the binary system given in Table 1 at a bubble point at 394 K.

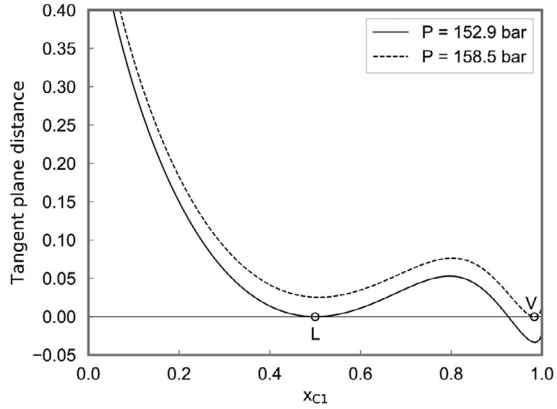

(b) Tangent place distance function defined at the equimolar mixture of methane/n-decane at a bubble point at 394 K.

Fig. 1. Gibbs free energy analysis for the equimolar mixture of methane/n-decane at a bubble point at 394 K in a 10-nm capillary tube. The L-phase pressure is 152.9 bar and the V-phase pressure is 158.5 bar.

Table 2
Critical properties for the methane/n-butane mixture used for Section 3.2.

Component	T_c	P_c	Acentric factor	Parachor	Binary interaction parameters	
	K	Bar			C1	n-C4
C1	190.7	46.0	0.008	74.05	0	0
n- C4	425.2	38.0	0.193	193.9	0	0

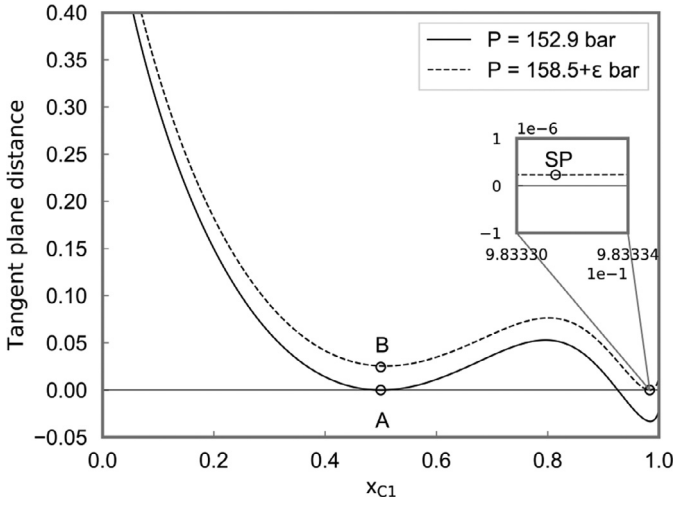

Fig. 2. Tangent plane distance curves for an equimolar mixture of methane and n-decane in a 10-nm capillary tube, at 394 K, at the bubble point oil pressure of 152.9 bar with a gas pressure of 158.5+ε bar.

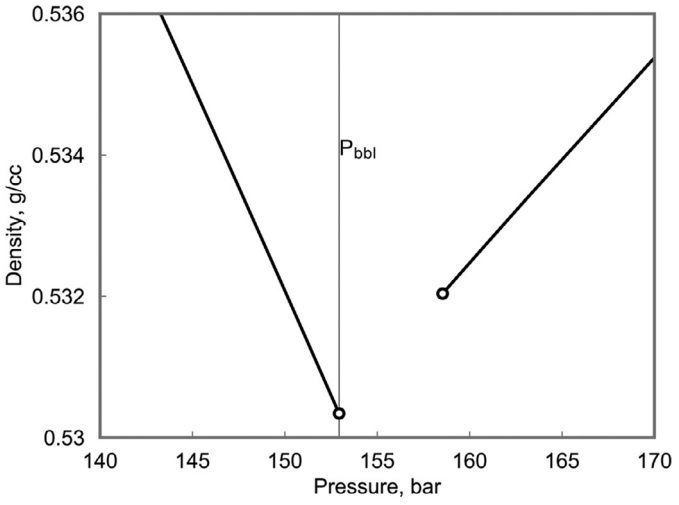

Fig. 3. Density of the L phase across the bubble point at 394 K for the equimolar mixture of methane and n-decane (Table 1) when the phase-split calculation is performed with a pressure specified for the V phase.

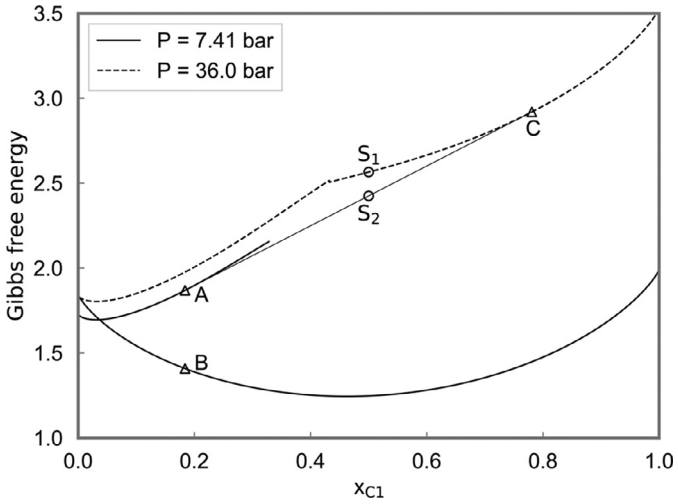

Fig. 4. Gibbs free energy curves of the methane/n-butane system (Table 2) at 36.0 bar and 7.41 bar at 333 K. The capillary tube radius is assumed to be 3 nm.

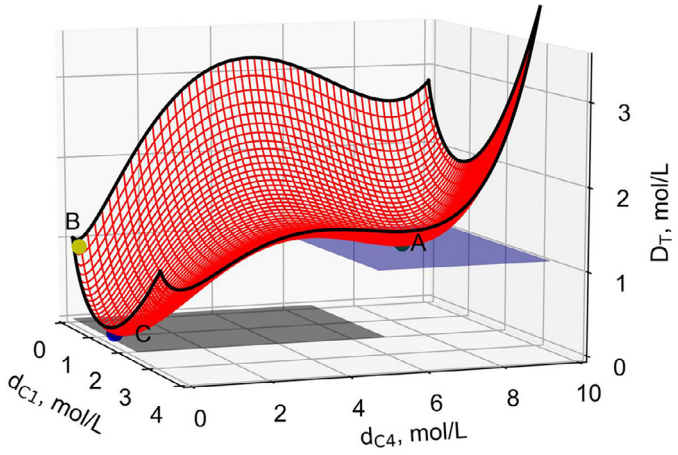

Fig. 5. \Tangent plane distance to the A/VRT function defined at point C (V phase in Fig. 4) at 333 K, 36 bar, and 78.1 mol% methane. The gray plane is the tangent plane at the V phase, which defines the basal plane in this figure. The blue plane is the tangent plane at the L phase and parallel to the gray plane. The D_T value for this blue plane gives P_{cap}/RT.

plane distance (D_T) defined at a reference phase, we use the D_T function (instead of A/VRT) defined as follows:

$$D_T = \left[\sum_{i=1}^{N_c} \left(\bar{G}_i - \bar{G}_{ir}\right) d_i - (P - P_r)\right] / RT, \tag{28}$$

where subscript "r" represents the reference phase. Fig. 5 shows D_T with the V phase (point C in Fig. 4) as the reference phase. The gray plane is the tangent plane at the V phase, which defines the basal plane in this figure. The blue plane is the tangent plane at the L phase and parallels to the gray plane. The D_T value for this blue plane gives P_{cap}/RT as explained in Achour [15] and Achour and Okuno [16]. Points A, B, and C are located on a single D_T surface. Note that A and B are on two different convex parts of D_T, indicating that these two points have different characteristics (or identities) as fluids. The possibility of two phases with points B and C is denied by both Eqs. (12) (or 13) and 14.

This figure clarifies that a robust root selection will avoid the switching from one side to another on the D_T plane for a given phase. This can be done by i) initialization of the two-phase split calculation by using a phase stability analysis algorithm that provides good initial guesses on the basis of minimization of the

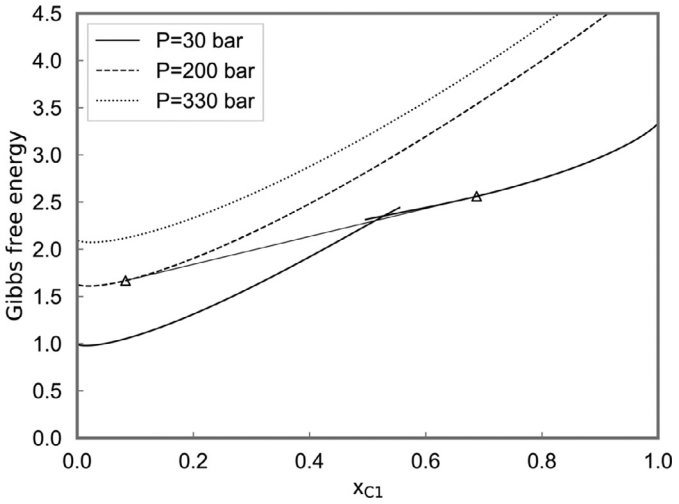

Fig. 6. Gibbs free energy curves for the methane/n-decane system at 300 K and 30, 200, and 330 bar. There is no equilibrium solution for the 60%-methane mixture with the L-phase pressure specified at 30 bars if the surface is liquid wet.

Helmholtz free energy [15-16]; and ii) consistent selection of the cubic EOS root when Eq. (14) is solved throughout the iteration.

3.3. Case 3: Indefinite solution using the conventional method

As described in the introduction section, a phase-split problem including capillary pressure may encounter the indefinite situation, in which the fluid is unstable as a single phase, but no solution exists for the phase-split calculation. The algorithm developed in this research is designed to detect and confirm such indefinite situations. It finds a limiting capillary pressure at which one of the phases is located on the spinodal boundary of the Helmholtz free energy (A/VRT) while satisfying Eqs. (13) and (14) with the capillary pressure identified. This confirms the indefinite situation by finding the limiting capillary pressure, beyond which no solution exists for the phase-split problem.

Fig. 6 shows the Gibbs free energy curves for the methane/n-decane system (Table 1) at 300 K at three pressures: 30 bars (solid curve), 200 bar (dashed curve), and 330 bar (dotted curve). Two types of failures of the traditional phase-split method using the Gibbs free energy are described below. In this case study, the capillary pressure is treated as a constant to simplify the explanation and for easy visualization.

First, there is no equilibrium solution for a mixture of 60% methane and 40% n-decane with the L-phase pressure specified at 30 bars if the surface is liquid wet. As can be seen in this figure, no common tangent line is possible between a point (L phase) on the curve at 30 bar and another point (V phase) on the curve at 200 bar or 330 bar. This indefinite situation has been known since 2001 [10], but may have been confused as a phase-stability problem [7]. As described below, it is more accurate to view it as the lack of an equilibrium solution at high capillary pressure because the stability as a single-phase fluid is denied by the second law of thermodynamics.

Fig. 7 shows the total Gibbs free energy for all possible two-phase configurations of 60% methane and 40% n-decane with no capillary pressure (Fig. 7a) and with a capillary pressure of 170 bar (Fig. 7b) at 300 K and a L-phase pressure of 30 bar. The Gibbs free energy of the hypothetically single-phase mixture is shown with a bold line in the figure. The V phase is assumed to be richer in methane than the reference mixture, giving a range of methane mole fractions from 0.6 to 1. The range of methane mole fractions for the L phase is only shown from 0 to 0.5 because the upper

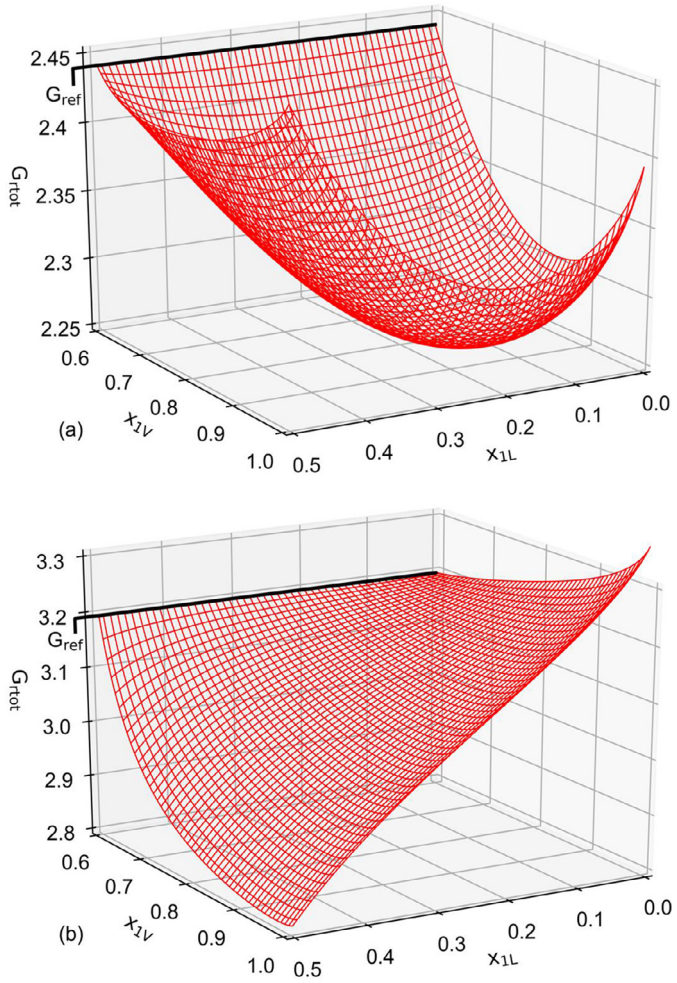

Fig. 7. Total Gibbs free energy for a mixture of 60 % methane and 40% n-butane with a liquid pressure of 30 bar with no capillary pressure (a), and with a gas phase pressure of 200 bar (b).

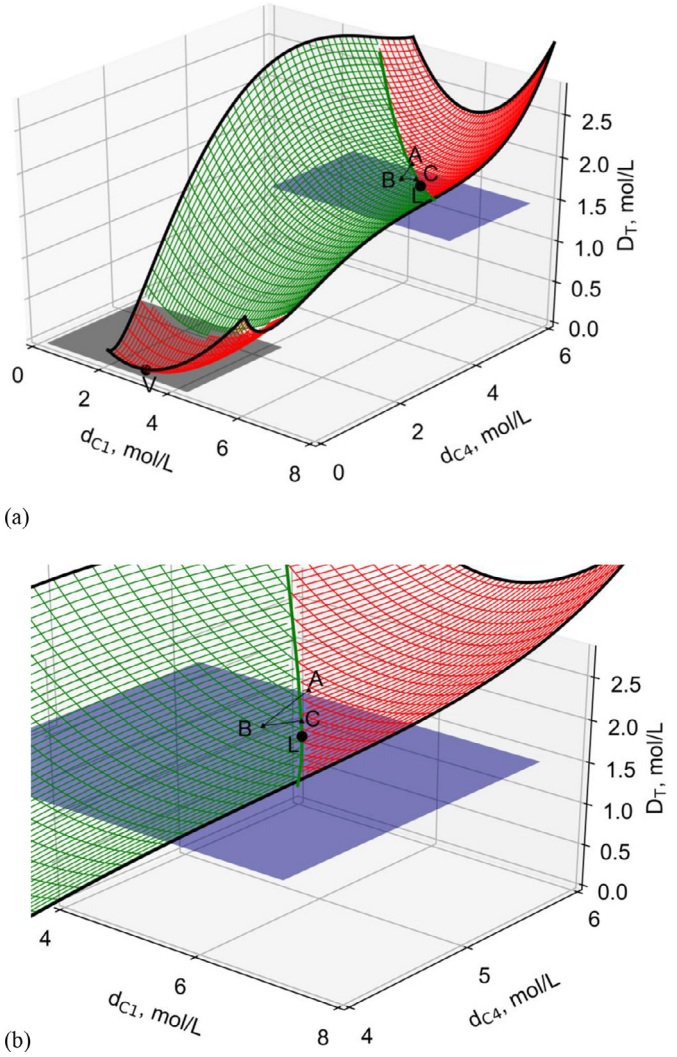

Fig. 8. Tangent plane to the Helmholtz free energy surface for the methane/n-decane system at 300 K and 0.1055 L/mol in a tube with a capillary radius of 0.1 nm. The solution is indefinite as a result of the capillary radius being overly small. The phase compositions (L and V) at convergence are represented by the two points on the Helmholtz free energy. For clarity, the region near the L phase in (a) has been magnified in (b).

limit corresponds to the edge of the oil branch of the Gibbs free energy curve at 30 bar (Fig. 6).

Fig. 7ab show that there are two-phase systems that have a smaller total Gibbs free energy than the hypothetically single-phase fluid. However, only the case with no capillary pressure has an equilibrium solution as given by the minimum (Fig. 7a). For the case of a capillary pressure of 170 bar, the Gibbs free energy surface does not have a minimum (Fig. 7b). This explains why there is no equilibrium solution for the binary mixture and why no common tangent line can be drawn from the 30 bar Gibbs free energy curve to the 200 bar one.

Second, if the capillary pressure is set to be 170 bar (i.e., the V-phase pressure is 200 bar), the phase-split calculation results in the common tangent line shown in Fig. 6. This erroneously gives an L phase at 69 mol% methane and a V phase at 8.4 mol% methane. This type of phase flipping can cause complete failures of compositional reservoir simulation [40].

Fig. 8 shows the D_T function using the V phase as the reference phase. The non-convex region is shown in green, and this intrinsically unstable region separates two convex regions for the L and V phases. Fig. 8 also shows the iterative steps for the equimolar mixture for a 0.1-nm tube. This example with an extremely small radius is to make the iteration steps clearer in this figure for illustration purposes. The L phase initialized at point A goes to point B after the update of capillary pressure, composition, and molar volumes. Point B is in the green region of non-convexity with a capillary pressure of 110.4 bar. The algorithm then adjusts the capillary pressure, repeats the volume update, and repositions the L phase from point B to point C on the spinodal boundary. With point C being the L phase, the capillary pressure is 79.79 bar. This adjustment is performed when any of the phases go to the region of non-convexity in the algorithm developed. In the case shown in Fig. 8, the convergence is achieved with an L phase at 48.0 mol% methane and a V phase at 92.6 mol% methane. This converged L phase is marked by a black dot, which is located on the spinodal boundary. The capillary pressure for this converged solution is 35 bar. This capillary pressure does not follow the capillary pressure model, which gives 356 bar. Hence, the algorithm concludes that this phase-split problem has an indefinite solution.

The separation of the convex regions of the Helmholtz free energy (or D_T in the above example) by the non-convex region gives a useful constraint for the phase-split calculation with capillary pressure. It does not seem possible to take a similar approach with the Gibbs free energy because different phases are located on different Gibbs free energy surfaces in pressure-composition space in the conventional phase-split method as shown in Fig. 6.

Table 3
Peng-Robinson EOS model for the equimolar mixture of Eagle Ford light oil and methane [41]. This fluid is used for Section 3.4.

	Composition	Molecular weight	Critical pressure	Critical temperature	Acentric factor	Parachor
	mole fraction	g/mol	bar	K		
N_2	0.00073	28.01	33.9349143	126.2	0.04	41
CO_2	0.01282	44.01	73.8431786	304.222222	0.225	78
C_1	0.31231	16.04	46.3944429	190.7	0.013	77.3
C_2	0.04314	30.07	48.8255536	305.427778	0.097	108.9
C_3	0.04148	44.1	42.5551214	369.888889	0.152	151.9
i-C_4	0.0135	58.12	36.46735	408.111111	0.185	181.5
n-C_4	0.03382	58.12	37.9562071	425.222222	0.201	191.7
i-C_5	0.01805	72.15	33.3269643	460.388889	0.2223	225
n-C_5	0.02141	72.15	33.7419143	469.783333	0.2539	233.9
n-C_6	0.04623	86.18	30.3078929	507.888889	0.3007	271
C_{7-10}	0.16297	112	27.7644286	589.166667	0.3739	311
C_{11-14}	0.12004	175	21.2093214	679.777778	0.526	471
C_{15-19}	0.10044	210	16.6393571	760.222222	0.6979	556.3
C_{20+}	0.07306	250	10.4151071	896.777778	1.0456	836.4

Table 4
Binary interaction parameters for the fluid shown in Table 3 [41]. This fluid is used for Sections 3.4.

	N_2	CO_2	C_1	C_2	C_3	i-C_4	n-C_4	i-C_5	n-C_5
N_2	0								
CO_2	-0.02	0							
C_1	0.036	0.1	0						
C_2	0.05	0.13	0	0					
C_3	0.08	0.135	0	0	0				
i-C_4	0.095	0.13	0	0	0	0			
n-C_4	0.09	0.13	0	0	0	0	0		
i-C_5	0.095	0.125	0	0	0	0	0	0	
n-C_5	0.1	0.125	0	0	0	0	0	0	0
n-C_6	0.1	0.125	0	0	0	0	0	0	0
C_{7-10}	0.151	0.11	0.025	0.02	0.015	0.01	0.01	0.005	0.005
C_{11-14}	0.197	0.097	0.049	0.039	0.029	0.019	0.019	0.01	0.01
C_{15-19}	0.235	0.085	0.068	0.054	0.041	0.027	0.027	0.014	0.014
C_{20+}	0.288	0.07	0.094	0.075	0.056	0.038	0.038	0.019	0.019

Table 5
Capillary pressure parameters used for Section 3.4, as given in Neshat et al. [8]. The permeability was reduced to 0.5 μD to make region II more apparent in Fig. 9.

γ	S_w	ϕ	k	b_o	b_g	a_o	a_g	S_{omin}	S_{gmin}
			μD						
3.88	0	0.045	0.5	0.1	-0.027	1.35	0.1	0.07	0.063

3.4. Case 4

This case study presents the convergence behavior of the algorithm developed in this research and illustrates the points made in the previous case studies using a more realistic fluid, an Eagle Ford light oil. The PR EOS model [41] is given in Table 3 and 4. Table 5 gives the parameters for the saturation-based capillary pressure model fitted the data for a tight rock [8]. The permeability was reduced from 9 μD to 0.5 μD to help illustrate the challenging convergence to indefinite solutions.

Fig. 9 shows the P-T phase envelope for the Eagle Ford light oil. The shaded regions I and II represent the conditions at which the dominant eigenvalue of the Jacobian (Appendices B and C) are smaller than −0.9. In those cases, the molar volume update and under-relaxation procedures are performed according to the procedure described in Section 2.2.4. We perform flash calculations along the isotherm at 350 K and show the convergence behavior of the algorithm at points A, B, and C. Points A and B are at 350 K.

Fig. 10 shows the results of the PT and TV flash calculations along the 350 K isotherm. The discontinuity in density occurs with PT flash, but not with VT flash. The magnitude of the discontinuity is smaller than in case 1 because it is equal to the capillary pressure at the phase boundary. The interfacial tension in this case is equal to 2.5 mN/m. To avoid this type of discontinuous phase behavior prediction needs flash calculations based on total molar volume instead of phase pressure.

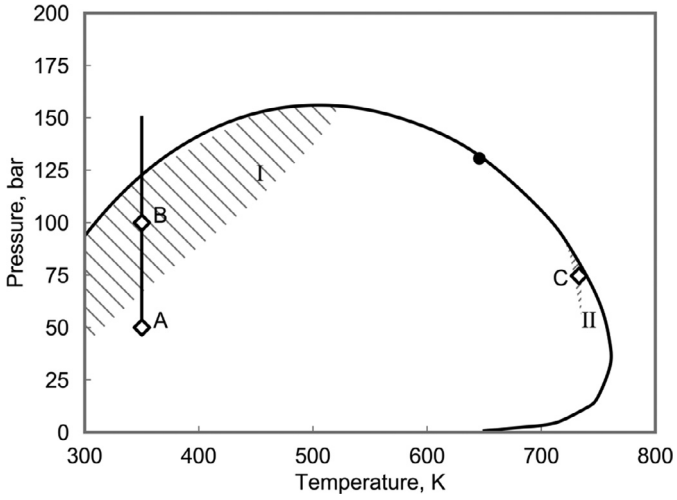

Fig. 9. Phase envelope for Eagle Ford light oil including the effect of a saturation-based capillary pressure. Regions I and II show the conditions where the dominant eigenvalues for the Jacobian matrices described in Appendices B and C satisfy the condition $\lambda_d < -0.9$, respectively. The vertical line represents the isotherm at 350 K along which the pressure-volume relation is computed using the PT and TV flash algorithms in Fig. 10. The convergence behavior of the algorithm for Points A, B, and C are shown in Figs. 10, 11, and 12, respectively.

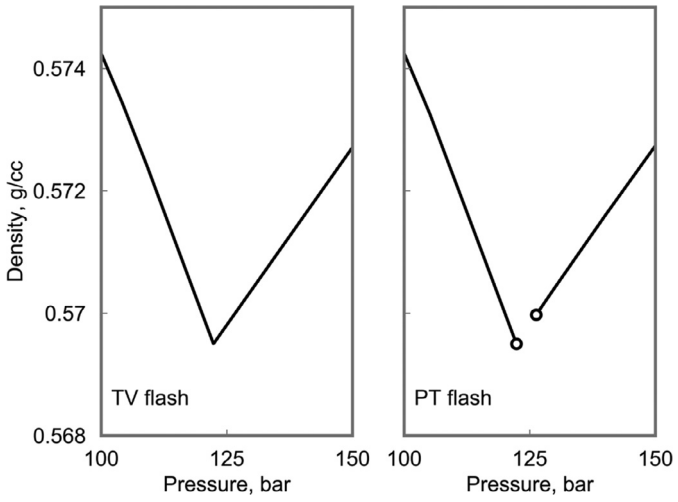

Fig. 10. Density of the L phase across the bubble point at 350 K for Eagle Ford light oil (Tables 3 and 4) when the phase-split calculation is performed using the V-phase pressure using the VT and PT flash algorithms.

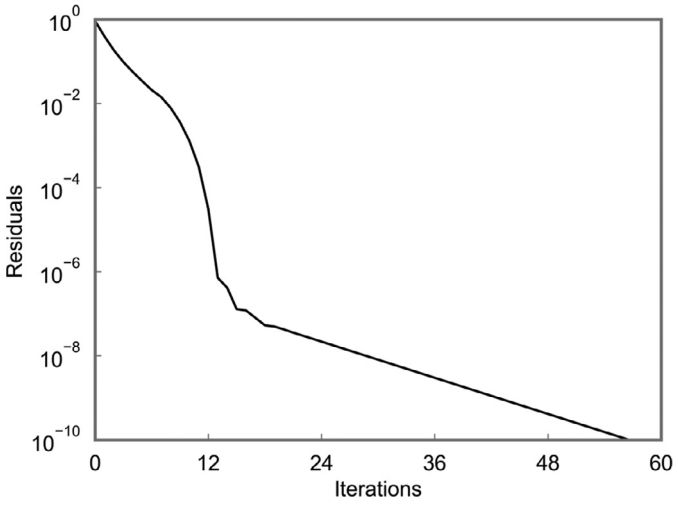

Fig. 11. Convergence behavior for the algorithm for Eagle Ford light oil (Tables 3 and 4) at 350 K and a total molar volume of 238.3 cc/mol. The L- and V-phase pressures at convergence are 50.00 bar and 64.75 bar, respectively. The L-phase pressure and temperature conditions are shown in Figure 9 as point A.

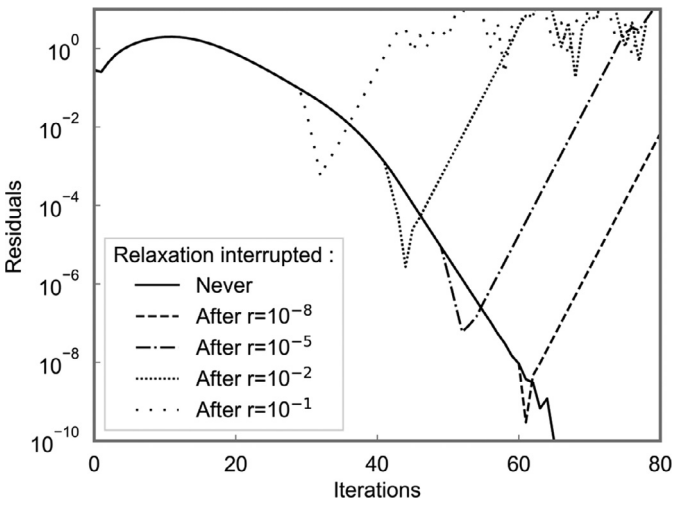

Fig. 12. Convergence behavior for the algorithm for Eagle Ford light oil (Tables 3 and 4) at 350 K and a total molar volume of 182.7 cc/mol. The L- and V-phase pressures at convergence are 100.0 bar and 105.4 bar respectively. The L-phase pressure and temperature conditions are shown in Fig. 9 as point B.

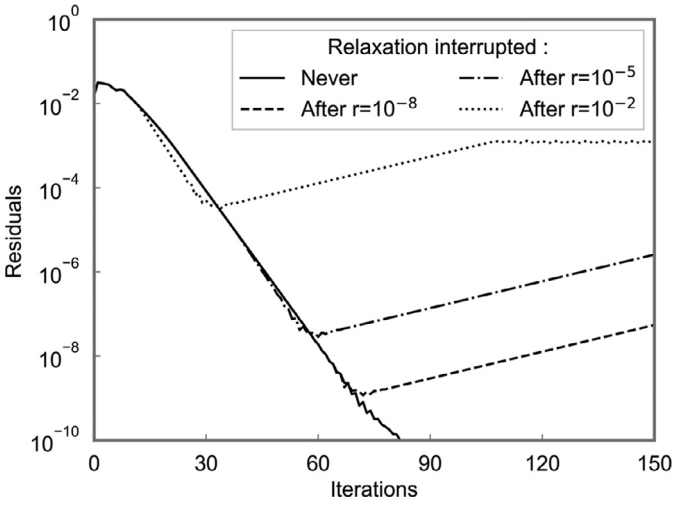

Fig. 13. Convergence behavior for the algorithm for Eagle Ford light oil (Tables 3 and 4) at 733 K and a total molar volume of 640.0 cc/mol. This is an example of indefinite solution, and the algorithm converges to the limit of indefiniteness by readjusting the molar volumes and capillary pressure during the iteration. The L- and V-phase pressures at convergence are 74.31 bar and 74.64 bar, respectively. The V-phase pressure and temperature conditions are shown in Fig. 9 as point C.

Fig. 11 shows the convergence behavior for the new algorithm at point A at 350 K for a molar volume of 238.3 cc/mol. The L- and V-phase pressures at convergence are respectively 50.00 and 65.75 bar. This figure shows that the residual converges linearly with two distinct slopes on the logarithmic scale. The slope change after 10 iterations is caused by the use of safety factors used in the under-relaxation when the residual is smaller than 10^{-3} (see Section 2.2.2). No under-relaxation was used when the residual was greater than 10^{-3} because the dominant eigenvalue of the Jacobian (Appendix B) is -0.65, which is greater than -0.9.

Fig. 12 shows the convergence behavior (solid line) for this algorithm at point B for a temperature of 350 K and a molar volume of 182.7 cc/mol. The L- and V-phase pressures at convergence are 100.0 and 105.4 bar, respectively. In this case, an under-relaxation factor of 0.586 is needed to converge to the correct solution because the dominant eigenvalue of the Jacobian (Appendix B) is -2.24. The dashed, dash-dotted, dotted, and loosely dotted line shows the convergence behavior when the under-relaxation routine is made inactive at $||F_i||_\infty \approx 10^{-1}$, 10^{-2}, 10^{-5}, and 10^{-8}. As soon as the under-relaxation is interrupted, the residual deviates from the original convergent behavior, and diverges. This divergence behavior was previously observed and reported by Jindrová and Mikyška [22] and Lu et al., [17] for flash calculation with and without capillary pressure. However, they neither presented any analysis of the divergence behavior, nor proposed systematic methods for convergence to the correct solution. It is essential to use the under-relaxation method developed in this paper.

This divergence behavior is caused by the increase of elements of matrix **B** (Appendix B) near the bubble point at low temperatures because of the inverse of the term $(\beta_L/(dP_L/d\underline{V}_L) + \beta_V/(dP_V/d\underline{V}_V))$. Near the bubble point, β_V approaches 0. At low temperatures, $dP_L/d\underline{V}_L$ and $dP_V/d\underline{V}_V$ increase. In general, the magnitude of the capillary pressure does not have a very strong effect on the size of region I.

Fig. 13 shows the convergence behavior for the new algorithm at point C for a temperature of 733 K and a molar volume of 640.0 cc/mol. The L and V phase pressures at the converged limit of indefinite solution are respectively 74.31 and 76.64 bar, giving

a capillary pressure of 0.33 bar (the capillary pressure given by the capillary pressure model is equal to 0.43 bar). In this case, an under-relaxation factor of 0.927 was needed to converge to the correct solution because the dominant eigenvalue of the Jacobian (Appendix B) is equal to -1.05. The same divergence behavior as Region I occurs when the relaxation is interrupted at any point in the algorithm.

4. Conclusion

The phase-split problem in the presence of capillary pressure was formulated using the Helmholtz free energy for a given temperature and total volume. The algorithm developed in this research is based on the successive substitution method for the K value update coupled with the volume update through the pressure constraint equation. Case studies demonstrated that the phase-split problem with capillary pressure can be more robustly solved by using the Helmholtz free energy than the Gibbs free energy. Conclusions are as follows:

- The traditional methods, which use the Gibbs free energy, can cause a discontinuity in phase properties across phase boundaries. This undesirable discontinuity occurs when the specified pressure is given to the V phase acrossa bubble pointand when it is given to the L phase acrossa dew point. No general solution exists for phase identification without a priori knowledge of phase behavior for the fluid of interest. This discontinuity problem does not occur with the algorithm developed in this research since total molar volume is continuous across a phase boundary and phase pressures are part of the solution.
- The fundamental reason for the improved robustness is that the algorithm involves only one energy surface regardless of the number of phases. The variability of phase pressures that occurs during the iteration is inherently considered in the Helmholtz free energy to be minimized for a given temperature and total volume. The robustness of the new algorithm was demonstrated for the cases in which the traditional method encounters convergence problems because of a non-physical part of the Gibbs free energy (e.g., the V-phase part of the Gibbs free energy at the L-phase pressure).
- A case study demonstrated that the new algorithm can detect and confirm the indefinite situation where the fluid is unstable as a single-phase fluid, but has no two-phase solution. For such an indefinite situation, the algorithm gives a capillary pressure with which one of the phases is located on the spinodal boundary while satisfying the fugacity equations and the pressure and mass balance constraints. The conventional method can either converge to an incorrect solution or result in non-convergence in such an indefinite situation.
- In the cases studied in this research, two equilibrium phases were found on two distinct regions of convexity on the Helmholtz free energy. The two convex regions were separated by a non-convex region of intrinsic instability. This topological information of the Helmholtz free energy was used to improve the robustness of the successive substitution.
- The convergence behavior of successive substitution was analyzed for flash calculation using the Helmholtz free energy, on the basis of the dominant eigenvalue of the Jacobian matrix. The analysis enabled the algorithm to avoid the divergence near bubble points at low temperatures, and at some conditions of indefinite solution.

Declaration of Competing Interest

The authors declare that they have no known competing financial interests or personal relationships that could have appeared to influence the work reported in this paper.

Supplementary materials

Supplementary material associated with this article can be found, in the online version, at doi:10.1016/j.fluid.2021.112960.

Appendix A: Flow chart for TV flash using the Helmholtz free energy

The flow chart below presents the detailed steps for the algorithm developed in this research as explained in Section 2.2. The flowcharts for the initialization steps and the procedure for solving the pressure equation at each outer-loop iteration are given in the supporting information.

Appendix B: Jacobian matrix for TV flash

This appendix presents a detailed description of the Jacobian used to evaluate the under-relaxation coefficient. The equations presented in this appendix contain many derivatives of the equation of state, for which the supporting information provides analytical expressions.

The Jacobian contains derivatives of **g** at a constant total molar volume. The constant total molar volume constraint can be satisfied by using the chain-rule

$$\left(\partial g_i/\partial t_j\right)_{\underline{V},t_{k\neq j}} = \left(\partial g_i/\partial t_j\right)_{P,t_{k\neq j}} + \left(\partial g_i/\partial P\right)_{\mathbf{t}}\left(\partial P/\partial t_j\right)_{\underline{V},t_{k\neq j}}, \tag{B1}$$

where $i = 1,\ldots,N_c$, $j = 1,\ldots,N_c$, and the derivative of pressure can be evaluated using chain rule again $(\partial P/\partial t_j)_{\underline{V},t_{k\neq j}} = -(\partial P/\partial \underline{V})_{\mathbf{t}}(\partial \underline{V}/\partial t_j)_{t_{k\neq j}}$.

The Jacobian can be split into four separate parts

$$\mathbf{J} = \begin{pmatrix} \mathbf{S} & \mathbf{v} \\ \mathbf{w} & u \end{pmatrix}, \tag{B2}$$

where $\mathbf{S} \in \mathbb{R}^{(N_C+1)\times(N_C+1)}$, $\mathbf{v}$ and $\mathbf{w} \in \mathbb{R}^{(N_C+1)}$. The **S** matrix

$$\mathbf{S} = \mathbf{I} + \left(\nabla^2_{TP}G_L + \nabla^2_{TP}G_V - \mathbf{B}\right)\mathbf{Q}^{-1} \tag{B3}$$

differs from Jacobian derived by [4] for the PT flash only by the **B** matrix.

In Eq. (B3), $\nabla^2_{TP}G$ is the isothermal isobaric Hessian of the Gibbs free energy containing elements $\partial^2 G/\partial N_i \partial N_j$ $(i, j = 1,\ldots,N_c)$ given in the supporting information. The elements of matrix **B** are expressed as

$$B_{ij} = (RT)^{-1}\left(\bar{V}_{iL} - \bar{V}_{iV}\right)\left(\bar{V}_{jL} - \bar{V}_{jV}\right)/(\beta_L/(dP_L/d\underline{V}_L) + \beta_V/(dP_V/d\underline{V}_V)) \tag{B4}$$

where i, j = 1,....,$N_C$and the elements of the Q matrix are

$$Q_{ij} = \partial \ln K_i/\partial N_{jL} = 1/\beta_V + 1/\beta_L - \delta_{ij}(1/\beta_L x_{iL} - 1/\beta_V x_{iV}) \tag{B5}$$

where i, j = 1,....,N_C. The elements of the vector **w** are

$$w_i = (RT)^{-1}\underline{V}_r \sum_{i=1}^{N_c}\left(\partial \mathcal{P}_{cap}/\partial N_{jL}\right)\left(\partial N_{jL}/\partial \ln K_i\right) \tag{B6}$$

where i = 1,....,N_C and the derivatives $(\partial N_{jL}/\partial \ln K_i)$ are equal to the ij elements of the matrix $\mathbf{Q}^{-1}$. The elements of the vector **v** are

$$v_i = -\underline{V}_r^{-1}\left[\left(\bar{V}_{iL} - \bar{V}_{iV}\right)\beta_V/(dP_V/d\underline{V}_V)/(\beta_L/(dP_L/d\underline{V}_L) + \beta_V/(dP_V/d\underline{V}_V)) + \bar{V}_{iV}\right], \tag{B7}$$

where $i = 1,\ldots,N_c$. The derivatives dV_V/dP are equal to $\beta_V/(dP/d\underline{V}_V)$. Finally, the element at the bottom right of the Jacobian matrix is

$$u = 1 - (d\mathcal{P}_{cap}/dP_L + d\mathcal{P}_{cap}/dP_V)(dV_V/dP)/(dV_V/dP + dV_L/dP) \tag{B8}$$

where i = 1,....,N_C.

Appendix C: Jacobian matrix for computing the limit of indefinite solution

This appendix presents a detailed description of the Jacobian used to evaluate the under-relaxation coefficient for the indefinite solution. The supporting information provides many derivatives of the equation of state required for evaluation of the Jacobian.

In the course of convergence to an indefinite solution, the capillary pressure is readjusted to the limit of indefiniteness, where the smallest eigenvalue of the Hessian matrix of the Helmholtz free energy is 0. Then, the only independent variables are the phase compositions through $\ln K_i$ ($i = 1, \ldots, N_c$). The Jacobian can then be expressed as

$$J_{ij} = \left(\partial\left(\ln K_i + \ln\left(f_{iL}\right) - \ln\left(f_{iV}\right)\right)/\partial \ln K_j\right)_{\ln K_{k\neq j},\lambda_{N_c}=0} \tag{C1}$$

where i, j = 1,....,N_C. An analysis of the eigenvalues and eigenvectors is necessary to compute the derivative along the direction of constant minimum eigenvalue λ_{N_c}. For a real symmetric Hessian $\nabla^2_\delta A$ with the smallest eigenvalue λ_{N_c} and corresponding eigenvector $\boldsymbol{v}$ [42], the differential of the smallest eigenvalue is

$$d\lambda_{N_c} = \boldsymbol{v}^{\mathbf{T}} d\left(\nabla^2_\delta A\right)\boldsymbol{v}. \tag{C2}$$

Along a line of constant eigenvalue, $d\lambda_{N_c} = 0$. In this research, the Hessian of the Helmholtz free energy $\nabla^2_\delta A$ is evaluated in $\boldsymbol{\delta}$-space because it is dimensionless. The analytical expressions for the Hessian is given in the Supporting information. The differentials for the Helmholtz free energy eigenvalue are evaluated in the variable space of number of moles and total volume

$$\sum_{i=1}^{N_c} \boldsymbol{v}^{\mathbf{T}}\left(\partial \nabla^2_\delta A/\partial N_{iL}\right)\boldsymbol{v} + \boldsymbol{v}^{\mathbf{T}}\left(\partial \nabla^2_\delta A/\partial V_L\right)\boldsymbol{v} = 0, \tag{C3}$$

which gives a derivative of the liquid volume along the constant minimum eigenvalue line

$$\left(\partial V_L/\partial N_{jL}\right)_{\lambda_{N_c}=0,N_{k\neq iL}} = -\left(\boldsymbol{v}^{\mathbf{T}}\left(\partial \nabla^2_\delta A/\partial N_{jL}\right)\boldsymbol{v}\right)/\left(\boldsymbol{v}^{\mathbf{T}}\left(\partial \nabla^2_\delta A/\partial V_L\right)\boldsymbol{v}\right). \tag{C4}$$

The elements of $\partial \nabla^2_\delta A/\partial N_{jL} = \partial^3 A/\partial\delta_k\partial\delta_j\partial N_{jL}$ and $\partial \nabla^2_\delta A/\partial V_L = \partial^3 A/\partial\delta_i\partial\delta_j\partial V_L$ can be evaluated analytically from the third-order derivative of the Helmholtz free energy in **N**-space

$$\partial^3 A/\partial\delta_k\partial\delta_j\partial N_{iL} = \left[\left(\partial^3 A/\partial N_i\partial N_j\partial N_k\right)\left(\sqrt{N_i}\sqrt{N_j}\right) + 1/(2N)\left(\partial^2 A/\partial\delta_k\partial\delta_j\right)\left(\delta_{ik}/x_i + \delta_{jk}/x_j\right)\right] \tag{C5}$$

where i, j, k = 1,....,N_C and the second-order derivative of pressure in **N**-space

$$\partial^3 A/\partial\delta_i\partial\delta_j\partial V_L = -\left(\partial^2 P/\partial N_i\partial N_j\right)\left(\sqrt{N_i}\sqrt{N_j}\right) \tag{C6}$$

where i, j, k = 1,....,N_C.

It is more convenient to evaluate the derivatives with respect to the number of moles of the liquid phase, and then multiply it with the inverse of the **Q** matrix (Appendix B) than the logarithm of K-values. Eq. (C1) can then be rewritten using the mole balance constraint and the volume balance constraint and Maxwell's relations

$$\mathbf{J} = \mathbf{I} + (RT)^{-1}\left(\nabla^2_N A_L + \nabla^2_N A_V - \mathbf{C}\right)\mathbf{Q}^{-1}, \tag{C7}$$

where $\nabla^2_N A$ is the Hessian of isothermal isochoric Helmholtz free energy evaluated in mole number space at constant volume, and the elements of matrix **C** are equal to

$$C_{ij} = \left(\partial V_L/\partial N_{jV}\right)_{\lambda_{N_c}=0,N_{k\neq jL}}\left(\left(\partial P_L/\partial N_{iL}\right)_{N_{k\neq iL}} + \left(\partial P_V/\partial N_{iV}\right)_{N_{k\neq iV}}\right). \tag{C8}$$

where Maxwell's relation can be used to obtain a simpler derivative of $\ln(f_{iL})$ with volume

$$\left(\partial \ln\left(f_{iL}\right)/\partial V_L\right)_{\mathbf{N}_L} = -(RT)^{-1}\left(\partial P/\partial N_{iL}\right)_{\mathbf{N}_L}, \tag{C9}$$

in terms of a derivative of pressure as given in the supplemental information.

References

[1] Todd, H. B., and Evans, J. G., 2016. Improved Oil Recovery IOR Pilot Projects in the Bakken Formation. Presented at the SPE Low Perm Symposium, Denver, Colorado, 5-6 May. doi:10.2118/180270-MS.

[2] J.A. Rivero, M.M. Faskhoodi, G.G. Ferrer, H. Mukisa, A. Zhmodik, Huff-and-Puff Enhanced Oil Recovery in the Liquids-Rich Portion of the Montney: Applications for Gas Condensates, in: Presented at the Unconventional Resources Technology Conference, Denver, Colorado, 2019, pp. 22–24, doi:10.15530/urtec-2019-979. July.

[3] J.A. Sorensen, L.J. Pekot, J.A. Torres, L. Jin, S.B. Hawthorne, S.A. Smith, L.L. Jacobson, T.E. Doll, Field Test of CO2 Injection in a Vertical Middle Bakken Well to Evaluate the Potential for Enhanced Oil Recovery and CO2 Storage, in: Presented at the Unconventional Resources Technology Conference, Houston, Texas, 2018, pp. 23–25, doi:10.15530/URTEC-2018-2902813. July 2018.

[4] M.L. Michelsen, The Isothermal Flash Problem.Part I. Stability, Fluid Phase Equilibria 9 (1) (1982) 1–19, doi:10.1016/0378-3812(82)85001-2.

[5] M.L. Michelsen, The Isothermal Flash Problem. Part II. Phase-Split Calculation, Fluid Phase Equilibria 9 (1) (1982) 21–40, doi:10.1016/0378-3812(82)85002-4.

[6] B. Yan, Y. Wang, J.E. Killough, A Fully Compositional Model Considering the Effect of Nanopores in Tight Oil Reservoirs, J. Petrol. Sci. Eng. 152 (2017) 675–682, doi:10.1016/j.petrol.2017.01.005.

[7] M. Rezaveisi, K. Sepehrnoori, G.A. Pope, R.T. Johns, Thermodynamic Analysis of Phase Behavior at High Capillary Pressure, SPE J. 23 (6) (2018) 1438–1451, doi:10.2118/175135-PA.

[8] S.S. Neshat, R. Okuno, G.A. Pope, A Rigorous Solution to the Problem of Phase Behavior in Unconventional Formations with High Capillary Pressure, SPE J. 23 (4) (2018) 1438–1451, doi:10.2118/187260-PA.

[9] S.S. Neshat, R. Okuno, G.A. Pope, Thermodynamic Stability Analysis of Multi-Component Mixtures with Capillary Pressure, in: Presented at the SPE Reservoir Simulation Conference, Galveston, Texas, 2019, pp. 10–11, doi:10.2118/193888-MS. April.

[10] A.A. Shapiro, E.H. Stenby, Thermodynamics of the Multicomponent Vapor-Liquid Equilibrium Under Capillary Pressure Difference, Fluid Phase Equilibria 178 (1-2) (2001) 17–32, doi:10.1016/S0378-3812(00)00403-9.

[11] B. Nojabaei, R.T. Johns, L. Chu, Effect of Capillary Pressure on Phase Behavior in Tight Rocks and Shales, SPE Reservoir Evaluation & Engineering 16 (3) (2013) 281–289, doi:10.2118/159258-PA.

[12] N. Siripatrachai, T. Ertekin, R.T. Johns, Compositional Simulation of Hydraulically Fractured Tight Formation Considering the Effect of Capillary Pressure on Phase Behavior, SPE J. 22 (4) (2017) 1046–1063, doi:10.2118/179660-PA.

[13] D.R. Sandoval, W. Yan, M.L. Michelsen, E.H. Stenby, Influence of Adsorption and Capillary Pressure on Phase Equilibria Inside Shale Reservoirs, Energy & Fuels 32 (3) (2018) 2819–2833, doi:10.1021/acs.energyfuels.7b03274.

[14] H. Sun, H.A. Li, A New Three-Phase Flash Algorithm Considering Capillary Pressure in a Confined Space, Chem. Eng. Sci. 193 (2019) 346–363, doi:10.1016/j.ces.2018.09.013.

[15] S.H. Achour, Phase Stability Analysis for Tight Porous Media with The Helmholtz Free Energy, the University of Texas at Austin, Austin, Texas, 2019 M.S.E. report.

[16] S.H. Achour, R. Okuno, Phase Stability Analysis for Tight Porous Media by Minimization of the Helmholtz Free Energy, Fluid Phase Equilibria 520 (2020) 1–17, doi:10.1016/j.fluid.2020.112648.

[17] C. Lu, Z. Jin, H.A. Li, A Two-Phase Flash Algorithm with the Consideration of Capillary Pressure at Specified Mole Numbers, Volume and Temperature, Fluid Phase Equilibria 485 (2019) 67–82, doi:10.1016/j.fluid.2018.12.002.

[18] J. Mikyška, A. Firoozabadi, A New Thermodynamic Function for Phase-Splitting at Constant Temperature, Moles, And Volume, AIChE J. 57 (7) (2011) 1897–1904, doi:10.1002/aic.12387.

[19] J. Kou, S. Sun, A Stable Algorithm for Calculating Phase Equilibria with Capillarity at Specified Moles, Volume and Temperature Using a Dynamic Model, Fluid Phase Equilibria 456 (2018) 7–24, doi:10.1016/j.fluid.2017.09.018.

[20] J. Kou, S. Sun, X. Wang, An Energy Stable Evolution Method for Simulating Two-Phase Equilibria of Multi-Component Fluids at Constant Moles, Volume and Temperature, Comput. Geosci. 20 (1) (2016) 283–295, doi:10.1007/s10596-016-9564-5.

[21] D.R. Sandoval, M.L. Michelsen, W. Yan, E.H. Stenby, VT-Based Phase Envelope and Flash Calculations in the Presence of Capillary Pressure, Indust. Eng. Chem. Res. 58 (13) (2019) 5291–5300, doi:10.1021/acs.iecr.8b05976.

[22] T. Jindrová, J. Mikyška, Fast and robust algorithm for calculation of two-phase equilibria at given volume, temperature, and moles, Fluid Phase Equilibria 353 (2013) 101–114.

[23] D.V. Nichita, New Unconstrained Minimization Methods for Robust Flash Calculations at Temperature, Volume and Moles Specifications, Fluid Phase Equilibria 466 (2018) 31–47, doi:10.1016/j.fluid.2018.03.012.

[24] Rachford Jr, H. H., J.D. Rice, Procedure for use of electronic digital computers in calculating flash vaporization hydrocarbon equilibrium, J. Petrol. Tech. 4 (10) (1952) 19 -3.

[25] R. Okuno, R.T. Johns, K. Sepehrnoori, A New Algorithm for Rachford-Rice for Multiphase Compositional Simulation, SPE J. 15 (2) (2010) 313–325, doi:10.2118/117752-PA.
[26] Z. Xu, R. Okuno, Numerical simulation of three-hydrocarbon-phase flow with robust phase identification, Presented at the SPE Reservoir Simulation Symposium (2015) 23–25 February.
[27] J. Bennett, K.A. Schmidt, Comparison of Phase Identification Methods Used in Oil Industry Flow Simulations, Energy & Fuels 31 (4) (2017) 3370–3379.
[28] Edited and With an Introduction by J.D. van der Waals, J.S. Rowlinson (Ed.) Dover Publications, Inc., New York, 1873. Edited and With an Introduction by1988.
[29] G.M. Wilson, A Modified Redlich-Kwong Equation of State: Application to General Physical Data Calculations, Presented at the 65th National AIChE Meeting, 1969.
[30] R.A. Heidemann, M.L. Michelsen, Instability of Successive Substitution, Indust. Eng. Chem. Res. 34 (3) (1995) 958–966, doi:10.1021/ie00042a032.
[31] O. Orbach, C.M. Crowe, Convergence promotion in the simulation of chemical processes with recycle-the dominant eigenvalue method, Can. J. Chem. Eng. 49 (4) (1971) 509–513.
[32] D.V. Nichita, Fast and Robust Phase Stability Testing at Isothermal-Isochoric Conditions, Fluid Phase Equilibria 447 (2017) 107–124, doi:10.1016/j.fluid.2017.05.022.
[33] R.L. Scott, P.H. van Konynenburg, Static properties of solutions.Van der Waals and related models for hydrocarbon mixtures, Discuss. Faraday Soc. 49 (1970) 87–97, doi:10.1039/DF9704900087.
[34] M. Cismondi, M.L. Michelsen, Global phase equilibrium calculations: critical lines, critical end points and liquid–liquid–vapour equilibrium in binary mixtures, J. Supercritic. Fluids 39 (3) (2007) 287–295, doi:10.1016/j.supflu.2006.03.011.
[35] D.B. Robinson, D.Y. Peng, The Characterization of the Heptane and Heavier Fractions for GPA Peng-Robinson Programs, Gas Processors Association Research Report (1978).
[36] A. Kumar, R. Okuno, Direct Perturbation of the Peng–Robinson Attraction and Covolume Parameters for Reservoir Fluid Characterization, Chem. Eng. Sci. 127 (4) (2015) 293–309, doi:10.1016/j.ces.2015.01.032.
[37] D.S. Schechter, B. Guo, Parachors Based on Modern Physics and Their Uses in IFT Prediction of Reservoir Fluids, SPE Reserv. Evaluat. Eng. 1 (3) (1998) 207–217, doi:10.2118/30785-PA.
[38] R. Okuno, Modeling of Multiphase Behavior for Gas Flooding Simulation, the University of Texas at Austin, Austin, Texas, 2009.
[39] C.H. Whitson, M.R. Brulé, in: Phase Behavior, 20, Monograph Series, SPE, 2000, pp. 110–116.
[40] S.S. Neshat, Compositional Three-phase Relative Permeability and Capillary Pressure Models Using Gibbs Free Energy M.S.E. thesis, the University of Texas at Austin, Austin, Texas, 2016.
[41] A. Orangi, N.R. Nagarajan, M.M. Honarpour, J.J. Rosenzweig, Unconventional Shale Oil and Gas-Condensate Reservoir Production, Impact of Rock, Fluid, and Hydraulic Fractures, Presented at the SPE hydraulic fracturing technology conference, 2011 24-26 January, doi:10.2118/140536-MS.
[42] J.R. Magnus, On differentiating eigenvalues and eigenvectors, Econometric Theory 1 (2) (1985) 179–191.